



## EXPLORING NEAR-FAULT DIRECTIVITY EFFECT IN PROBABILISTIC SEISMIC HAZARD ASSESSMENT

Y. Chen<sup>(1)</sup>, M. Pagani<sup>(2)</sup>, G. Weatherill<sup>(3)</sup>, F. Cotton<sup>(4)</sup>

(1) Ph.D. Candidate, ROSE Programme, UME School, IUSS-Pavia, Italy, [yenshin.chen@globalquakemodel.org](mailto:yenshin.chen@globalquakemodel.org)

(2) Hazard Coordinator, Global Earthquake Model Foundation, Italy, [marco.pagani@globalquakemodel.org](mailto:marco.pagani@globalquakemodel.org)

(3) Senior Hazard Scientist, Global Earthquake Model Foundation, Italy, [graeme.weatherill@globalquakemodel.org](mailto:graeme.weatherill@globalquakemodel.org)

(4) Professor, Potsdam University and GFZ German Research Centre for Geosciences, Germany, [fcotton@gfz-potsdam.de](mailto:fcotton@gfz-potsdam.de)

### **Abstract**

Near-fault directivity effects can produce ground motions with high-amplitude, short duration pulses, which may cause serious damage to structures and buildings. Their prediction has important implications in the design of earthquake resistant structures. Prompted by the NGA-West2 project, several directivity models that aim to provide a more accurate estimate of hazard values – possibly in a probabilistic framework - have been recently proposed. To model the near-fault directivity effect in a probabilistic seismic hazard analysis (PSHA) framework, it is necessary to account for the aleatory variability of the hypocentral location and slip angle (for certain models) on each rupture generated by each fault source at close distance from the investigated site. This is a modeling approach not regularly considered in the more conventional PSHA practice, since the location of the hypocenter is rarely used in modern ground motion prediction equations (GMPEs).

We implemented into the OpenQuake-engine (an open software for seismic hazard and risk assessment) some of the most recently published directivity models and we extended the ordinary hazard integral by adding two additional aleatory variables, hypocenter location and slip angle, to support the near-fault directivity effect PSHA calculation.

Using a sample scenario based on an eighty-kilometer strike-slip fault and fixing as a reference the hazard values computed without accounting for the directivity effect, we observe at some sites surrounding the fault an increase of the values of ground motion up to 65 % at both 2 % and 10% probability of exceedance in 50 years. The discrepancy indicates the importance of considering the near-fault effect into the analysis for near-fault sites. As many major urban areas worldwide, such as San Francisco and Istanbul, are exposed to hazard caused by large faults with short distances. In this contribution, we describe the outcomes of some sensitivity analyses on the hazard results based on various distribution of the hypocentral location and fault geometries. We find that the hypocenter location has a strong impact on the hazard results, especially for scenario calculation, and that an over-simplified fault geometry model produces results which should be considered carefully while performing near-fault directivity PSHA.

*Keywords: PSHA; directivity effect, near-fault*

## 1. Introduction

The near-fault directivity effect is a modification in amplitude of the ground motion observed in proximity to the rupture and caused by the propagation of the rupture front at velocities close to the propagation of shear wave velocity in the encompassing rocks. When this condition is satisfied, the energy from the rupture when it arrives at the site is compressed in a small time interval. The result is that near-fault ground motions display characteristics that are different from ordinary ground motions since they often contain high amplitude, short duration pulses that can cause serious damage to structures and buildings [1–3].

Directivity effects have been clearly observed in many past events, including the 1971 San Fernando, California, the 1994 Northridge, California, the 1995 Kobe, Japan, the 1999 Chi-Chi, Taiwan, and the 2015 Gorkha, Nepal earthquakes. The amplification of near-fault ground motions caused by source rupture directivity effects produced severe damages to structures and buildings leading to fatalities and considerable economic loss. Therefore, accurate characterization of directivity in ground motion modelling has important implications for the design of earthquake resistant structures, especially those forming parts of critical infrastructures (i.e. lifelines, nuclear power plants).

Since the pioneering work of Somerville et al. [1] various physical and empirical models to quantify the near-fault directivity effect into probabilistic seismic hazard analysis (PSHA) have been proposed. The directivity effects can be modeled either with kinematic or dynamic models of calibrating with empirical model or purely driven by empirical data and that in this paper we will focus on the latter since they can be more efficiently incorporate in a PSHA framework. Many of them incorporate the rupture directivity term as a “post hoc” correction factor, which is usually a function of magnitude, source-to-site geometry, and frequency into ground motion prediction equations (GMPEs). More recent works [2–10] have expanded upon these approaches for modelling the near-fault rupture directivity effect into seismic hazard evaluation by incorporating more rupture physics (such as hypocenter location, rupture area, rupture direction), and seismological constraints to the predicted ground motion based on theory (e.g. isochrone theory) as well as on additional near-fault ground motion data.

Among the various directivity models described in the current literature, the dissimilar description of the term “directivity” should be noted; this requires care when applying these models in seismic hazard analysis. One source of confusion may be the inconsistent terminology of the term “directivity” in the engineering community and the seismology community. In the seismological literature, “directivity” exclusively relates to the finite fault rupture propagation effects. However, in the engineering literature, it indicates the combined effect of rupture propagation, earthquake source radiation pattern, ground motion directionality occurring at the near-fault sites [6], or it may relate exclusively to pulse-like ground motions observed at near-fault sites that are believed to be related to near-fault directivity effect [1, 3, 4, 6, 7].

Near-fault ground motions, especially the pulse-like ground motion, attract most of the attention in earthquake engineering community, due to the extreme demands they can place on structures. Mena and Mai [11], suggest that the generation of near-fault directivity pulses are strongly affected by the fault geometry and the asperity distribution along the fault plane. The directivity pulses are more likely to be observed at a site when the rupture propagates through the high-slip zone on the fault plane towards to the sites. However, the precise slip distribution is typically considered to be an aleatory variable, thus an explicit prediction of this information in PSHA is not currently possible. In the current practice, two main strategies have been proposed in the construction the seismic hazard models accounting for near-fault directivity [12]. One is to exclusively model probability of observing particular pulse effects based on purely empirical observation, and explicitly incorporate the likelihood of experiencing pulse motion at sites in a seismic hazard framework [e.g. 3, 9, 10]. The alternative strategy is based on the explicit characterization of the physical properties of the rupture in order to capture the azimuth-dependent changes in the ground motion amplitude and duration due to the rupture behaviour on the fault. Directivity in this second case corresponds to the cumulative effect of the finite fault rupture propagation, the radiation pattern and the ground motion particle polarization, as usually used in the engineering literature [e.g., 1, 2, 8, 9].

In our work, we explore the use of two recently published directivity models developed according to the two different strategies: empirically-derived versus physically characterized. These models were developed as

part of the NGA-West2 directivity project [8] to explore the impact of various choices on directivity models for PSHA. The first model is that of Shahi and Baker, (hereafter, SB13 model) [7] which exclusively targets at the pulse features. The second is the model proposed by Chiou and Spudich (hereafter, CS14 model) [8], which explicitly models the general directivity rupture effect. The two models are designed to be explicitly included into GMPEs. In this case their coefficients are determined simultaneously with all the other GMPE coefficients, instead of applying a “post hoc” correction to the median of a GMPE, by fitting directivity functional forms to the residuals of the GMPE.

Accounting for the near-fault directivity effect can be relevant in various typologies of analyses such as deterministic seismic hazard analysis (DSHA), probabilistic seismic hazard analysis (PSHA) [2] and near-real time ShakeMap [14] applications, to capture the ground motion spatial variability in the near-source once the properties of the source rupture have been defined.

The purpose of the paper is to illustrate the potential issues encountered when incorporating the aforementioned seismic source rupture directivity models explicitly in a PSHA framework. We highlight the potential limitations of the models and the sensitivity of the final hazard result to the choice of directivity model and its corresponding the source rupture assumptions.

## 2. Near-fault directivity PSHA implementation in OpenQuake-engine

To perform near-fault directivity PSHA in the OpenQuake-engine (an open-source software for seismic hazard and risk assessment) [15], two additional parameters are needed for characterizing the rupture behaviour: i.) a hypocenter distribution, in the form of a set of along-strike and down-dip locations with associated probabilities, and ii) slip distribution describing a set of slip angles and their associated probabilities. In current practice, it is challenging to specify rupture behaviour on faults even for the most well-studied fault systems; some studies have suggested that the hypocenter location distribution depends on the slip type and magnitude [16, 17]. Before applying a detailed hypocenter location distribution into the analysis, we explore the impact of the hypocenter location distribution on the resulting hazard curves (see section 3).

### 2.1 Two directivity models used in the study

In our work, we have implemented two directivity models- Chiou and Spudich model [8], and Shahi and Baker model [7] in OpenQuake-engine. Both models are “narrow-band”, in that the spectral amplification at a given period is functionally dependent on earthquake magnitude [18] and they are designed to be explicitly included into GMPEs, and until now, are the only two directivity models to have been explicitly included into available published GMPEs. The GMPE which includes the Chiou and Spudich directivity model is the Chiou and Youngs 2014 GMPE [19] (hereafter CY2014), whilst the Shahi and Baker directivity model is included into the GMPE developed by Shahi [7] (hereafter SB2013). Both models support the correction for strike-slip, and dipping fault type. However, bending faults (i.e. those whose angle of strike changes along the trace of the fault) is only supported for the CS14 model in our study; the literature we collected does not discuss the use of a bended fault in combination with the SB13 model.

#### 2.1.1 Chiou and Spudich 2014 directivity model (CS14)

The CS14 model is built upon the isochrone theory to predict the azimuthal distribution of shaking around a source. The predictor variables used in CS14 model are the slip distribution (nearly uniformly distributed), the finite fault radiation patterns and the seismic rupture propagation directivity (represented here by the isochrone velocity) [6, 8]. Using isochrone theory to model the rupture propagation, it follows that if all the energy radiated between the hypocenter and the direct point (the effective fraction of the hypocenter to target site distance that occurs on the rupture plane itself) arrives in a short time interval (higher isochrone velocity), then the energies are time-compressed and, thus, a directivity pulse is formed and the spectral amplitudes amplified. One main limitation of the CS14 model is that the model is not applicable for modelling strongly unilateral ruptures [4] for this reason the hypocenter must be at a distance from the rupture edge larger than 10%

of the fault length. Also, the model is not applicable for the cases where the rupture velocity approaches the S-wave velocity, since the ratio of rupture velocity to shear wave velocity is fixed at 0.8 in the model.

### 2.1.2 Shahi and Baker 2013 directivity model (SB13)

The SB13 model exclusively focuses on capturing the pulse-like features in ground motions at near-fault sites. Calibrated from the NGA-WEST2 dataset [20], the model computes the probability of observing a directivity pulse, the corresponding pulse period and pulse amplitude. Since the SB13 models the specific source effect-pulse like motion, the correction introduced is within a very narrow band which has peak at a period dependent to the magnitude of the earthquake. Pulses are expected to be observed only near to fault ruptures; hence, the SB13 model can be observed within a distance range significantly shorter than the one admitted by the CS14 model (this appears clearly in the test hazard map examples in Fig. 5, 6, 7). For PSHA calculation, the SB13 model requires only a hypocenter distribution (in strike-slip cases, the focal depth information will be neglected in the model)

## 3. Directivity-introduced amplification prediction results

We compute the amplifications of the median ground motion introduced by directivity effects computed from CY2014 (incorporating the CS14 directivity model), and SB2013 (incorporated with SB13 directivity model) respectively, in a controlling scenario with an eighty kilometer pure strike-slip fault of Mw 7.2 on spectral accelerations at T=2s, under various hypocenter assumptions for both models (Fig. 1). The amplification is computed as follows

Directivity induced amplification

$$= \frac{\text{median ground motion predicted from a GMPE with directivity term}}{\text{median ground motion predicted from a GMPE without directivity term}} \quad (1)$$

As already observed, this simple calculation confirms that the CS14 directivity model has a much broader effective correction range than the SB13 directivity model, since the CS14 model modifies the ground motion spatial variation around the fault caused by rupture propagation effect, whereas the SB13 model considers only the pulse-like ground motion that are observed at very near fault sites. The strengths of the ground motion spatial variation introduced by directivity in two models are diverse as well. The spatial ground motion variation is much stronger in CS14 model than in SB13 model. In both models, the results are significantly dependent on the hypocenter location for each deterministic test scenarios. In the next section, we will investigate the impact of various hypocenter distributions on PSHA results in order to understand the sensitivity to the hazard product while different hypocenter distribution assumption applied. In Fig. 1 (first row), we see that the amplification introduced by directivity is sensitive to the slip-direction assumption. The directivity effect is less pronounced when the slip direction is more away from the fault strike direction.

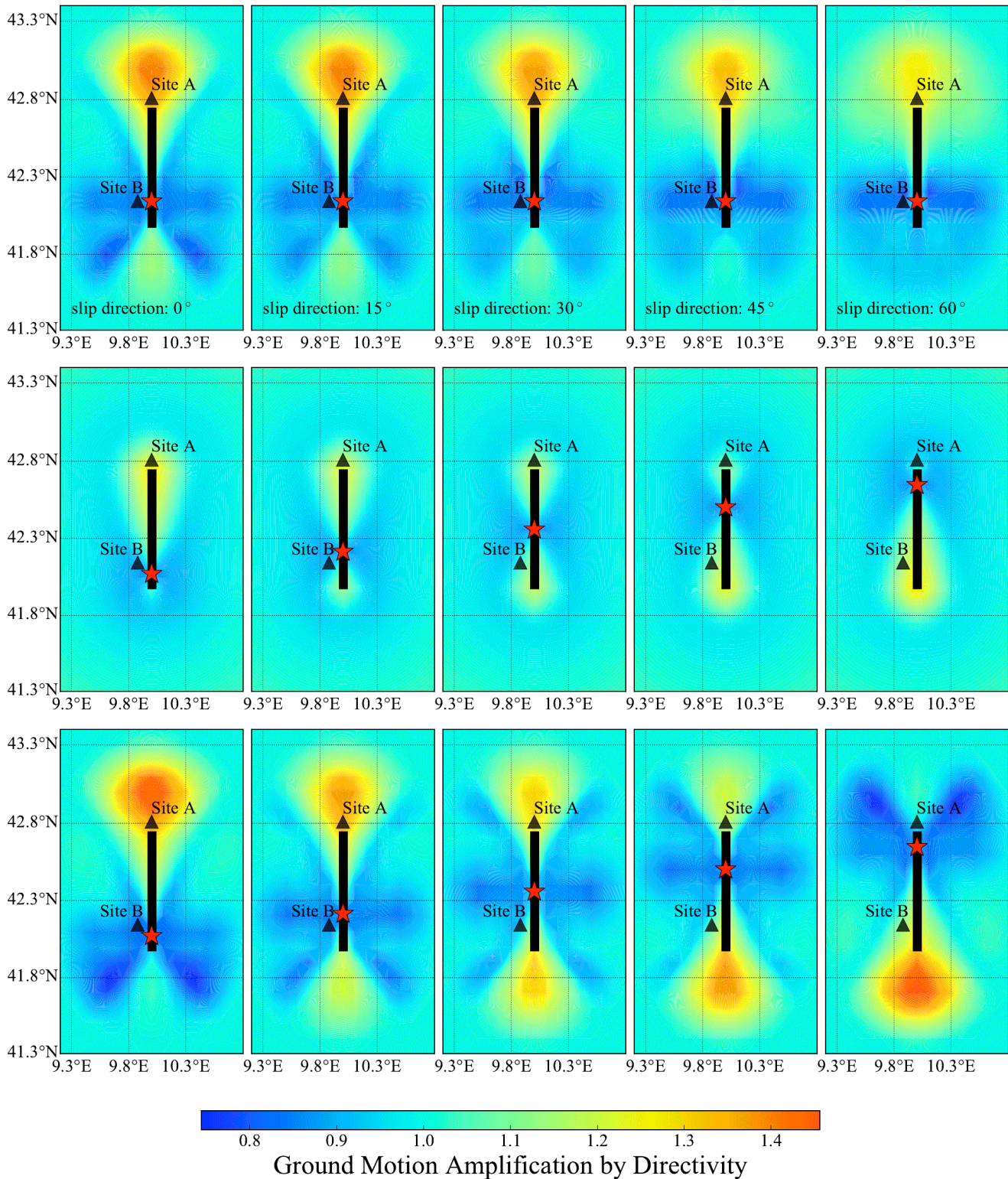


Fig. 1 - Amplification of ground motion due to rupture directivity in CY2014 GMPE (the first and third row) and SB2013 GMPE (the second row) for spectral acceleration ( $T=2$  sec.) computed considering an eighty kilometer long strike-slip rupture of Mw 7.2. The black line indicates the fault trace. The red stars represent hypocenter locations. Two test sites, A and B, shown as black triangles, will be used in the following hypocenter location sensitivity analysis. For the demonstration in bottom row, the slip direction is set up as fault strike direction (slip direction is  $0^\circ$ ).

The upper row exhibits the ground motion spatial variation with various slip direction from 0° to 60° with a step of 15°. The slip direction is defined here as the angle away from the horizontal within the fault plane (rake). The bottom row of Figure 1 demonstrates the ground motion spatial variation while the hypocenter location moves along the fault trace. Note that for all the analyses involving the CY2014 model, the slip direction corresponds to rake angle of the fault.

### 3. Sensitivity analysis of hypocenter location distribution in PSHA

As demonstrated in Fig. 1, the location of hypocenter controls the strength of the directivity effects in the computed ground motion fields. Before diving into near-fault PSHA and exploring the impact of different hypocenter distribution models, we investigate how the various hypocenter locations impact on PSHA result. For this purpose we perform a hypocenter location sensitivity analysis with ten test cases using the same fault scenario shown in Fig. 1, and observing the ground motion at the two test sites which are both 10 km away from the fault trace. Site A is located along the fault trace direction while site B sites is 10 km away from the rupture in a direction perpendicular to the trace. The first nine test cases consider a single hypocenter while for the test case 10, a uniform distribution of nine equally weighted hypocenter locations is considered. Uniform hypocenter distributions are commonly assumed in practice when considering near-fault directivity in PSHA.

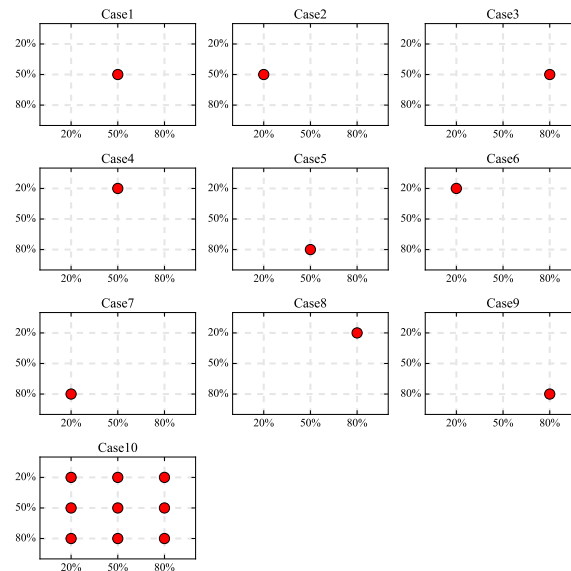


Fig. 2 - Hypocenter configurations used for sensitivity test. Each box represents a rupture plane, and the red dots indicate the position of the hypocenter on a rupture plane. For example, in the case 1 the hypocenter is placed along the strike at 50% of the fault length and at 50% of the fault width along the dip. For case 10, nine possible hypocenters are admitted for a rupture, and all the weights assigned on the hypocenters are equal weighted within the rupture as a non-informative case.

We compute the uniform hazard spectrum (UHS) at the two test sites for a 10% and 2% probability of exceedance (PoE) in 50 years for the case in which near-fault directivity considered (Figure 3), and for the case in which it is not explicitly considered (Figure 4). A  $M_w$  7.2 characteristic magnitude is assumed on the fault. In, a following analysis we will compute hazard maps for the same fault using classical PSHA and ruptures with magnitude in from 6.5 to 7.5 using truncated Gutenberg-Richer law with a value as 4.2 and b value set up as 0.9 (the predicted ruptures will float along the entire fault plane) (Fig. 4 and Fig. 5). In order to show the contribution of the hazard level introduced by near-fault directivity effect respect to the ordinary calculation, all

the result we show in the following are presented in the relative difference (Eq. 2) between the calculations with directivity included and the ones without.

$$\text{Relative difference} = \frac{\text{calculation with directivity included} - \text{ordinary calculation}}{\text{ordinary calculation}} \times 100\% \quad (2)$$

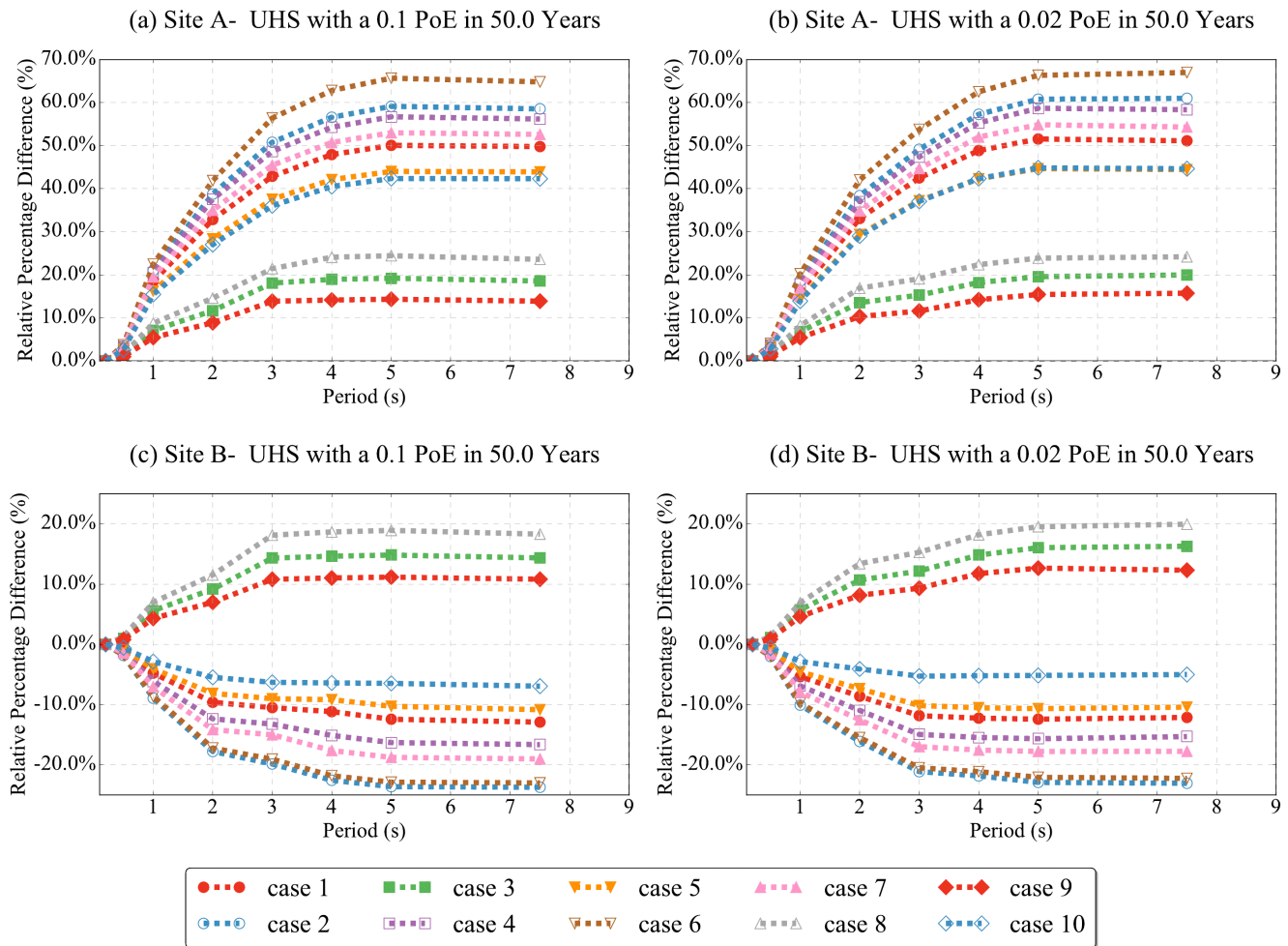
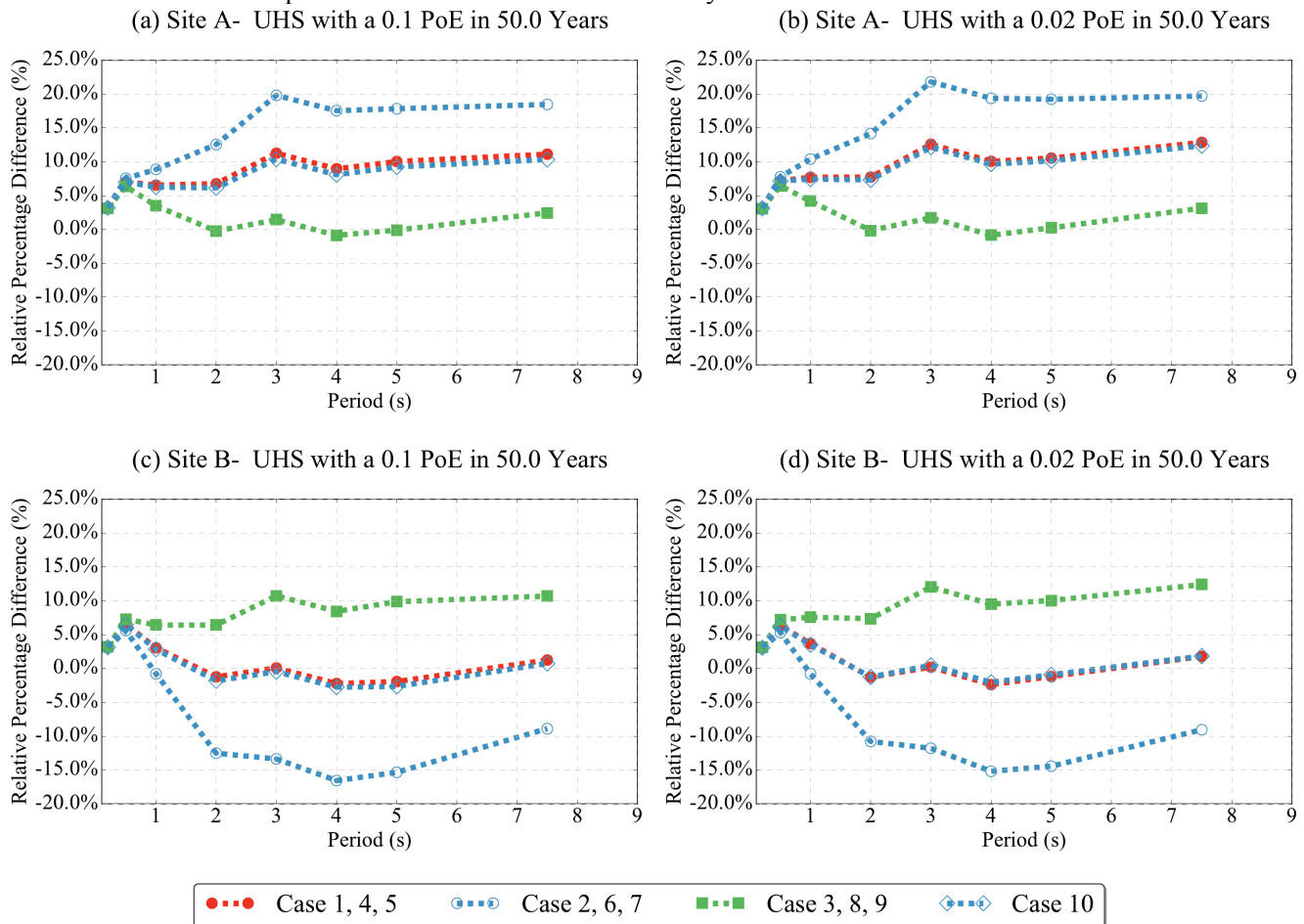


Fig. 3 - Relative percentage difference (%) of uniform hazard spectrum computed including near-fault directivity with the CS14 directivity model and the ordinary uniform hazard spectrum computed with the same GMPE but with the directivity effect turned off. Left column: UHS with 10% probability of exceedance (PoE) in 50 years. Right column: UHS with 2% probability of exceedance (PoE) in 50 years.

For the CS14 model, the directivity effect gets stronger with increased spectral acceleration periods, while it is relatively minor for short periods. For SB13 model, since the model focus on the pulse features, the correction arrives the maximum at certain period, which is the predicted pulse period. In our Mw 7.2 test source scenario, the median pulse period is predicted at around 3 second (Fig. 3 and Fig. 4).

In agreement with the observed ground motion field amplification introduced by directivity (Fig. 1), the CS14 model shows a much stronger directivity effect than SB13 model for all the test cases. Different approaches are used in the two models to account for the effective rupture fraction between the sites and the rupture nucleation point, the CS14 model is much more sensitive to the hypocenter location assumption on the hazard result than SB13 model. The difference among the hypocenter location test cases for CS14 model can be up to about 50% for the site located along the fault strike direction. The SB13 model appears less sensitive but the difference can also go up to about 20%. In general, if the site is located along the fault strike direction at

near-fault distance, we expect amplification introduced by directivity for both models but with various values of amplification. If the site locates aside to the fault trace, then the amplification magnitude strongly depends on the relative location of hypocenter and target sites. In general, if the target sites project onto the fault plane close to hypocenter location, we expect a de-amplification with respect to the ordinary calculation. For example, at test site B, most of the test cases showing de-amplification (case 2, 6, 7) are those for which the distance between hypocenter to the sites projection points onto the fault are shortest especially for case 2 in CS14 model. In CS14, the maximum de-amplification can reach around 25%, whilst, the sites which have longer distance between hypocenter and the site projection points on the fault (case 3, 8, 9) show that amplification can be up to almost 20%. One interesting observation for both models, is that the test case 5 and test 10 for both test sites show the very similar results. This suggests that when performing near-fault PSHA, a single hypocenter located as test case 5 might be a simplified – and calculation efficient - representation of the uniform hypocenter distribution. The results for different probabilities of exceedance are nearly identical.



**Fig. 4** - Relative percentage difference (%) of uniform hazard spectrum computed by adopting the SB13 directivity model and the ordinary uniform hazard spectrum at 10% and 2% probability of exceedance (PoE) in 50 years for sites A, B (see Fig. 1)

We then consider the same fault but with a magnitude distribution ranging from  $6.5 \leq M_w \leq 7.5$ , for which the predicted ruptures will be distributed (“floated”) along the entire fault plane. Now, the two types of hypocenter location used are those adopted in case 5 and case 1; the corresponding hazard maps for the 2 % probability of being exceeded in 50 years are shown in Figures 5 and 6 respectively. Overall, the hazard map results from both hypocenter assumptions are indeed quite similar, as we concluded in the previous observation, but only at the non-informative case (case 10), the result seems slightly smoother than the single hypocenter (case 5) especially for the CS14 model.

## 5. Sensitivity analysis of resampling fault geometry

Faults in the natural world are geometrically complex, yet most of the seismological models tend to assume planarity (or multi-planarity) in the geometrical description of the rupture. However, while dealing with near-fault seismic hazard evaluation, the result can be significantly dependent on the approximation rupture geometry. To understand the impact, we perform a sensitivity test using the example of a PSHA calculation to assess the hazard posed to Istanbul by large earthquakes on the northern branch of the North Anatolian Fault (NAF) in the Sea of Marmara.

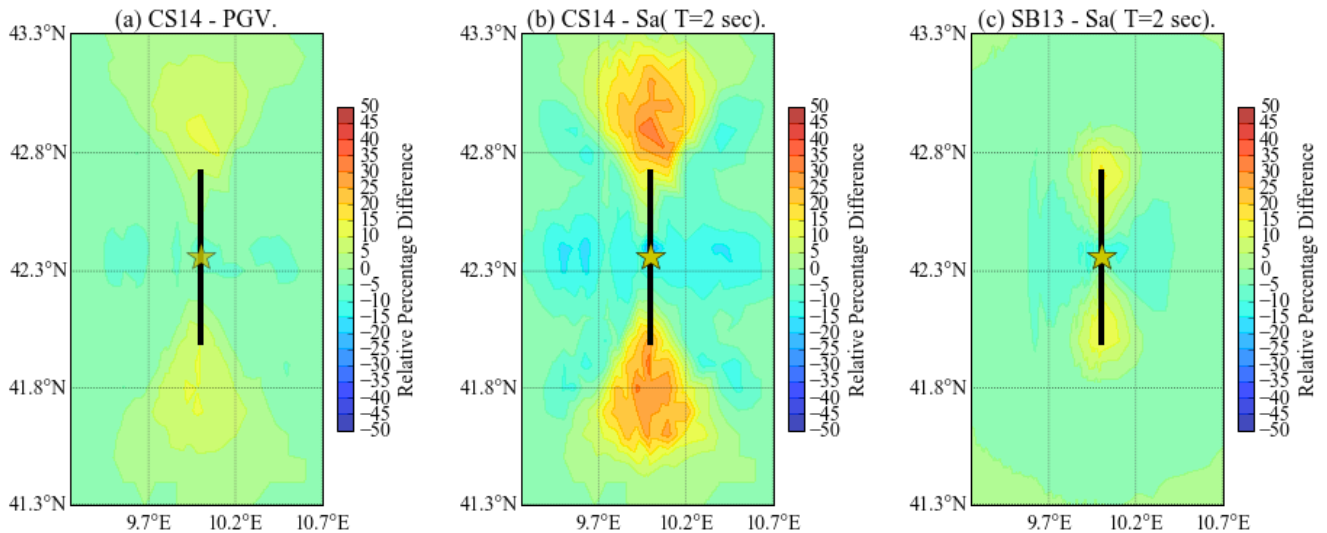


Fig. 5 - Relative percentage difference (%) of hazard map includes near-fault directivity calculation and the ordinary uniform hazard spectrum at 2% probability of exceedance (PoE) in 50 years for CS14 directivity model at PGV, Sa( T=2 sec.), and SB13 directivity model at Sa( T=2 sec.) for a strike-slip controlling scenario with the hypocenter location demonstrating in case 5 (see in Fig. 2).

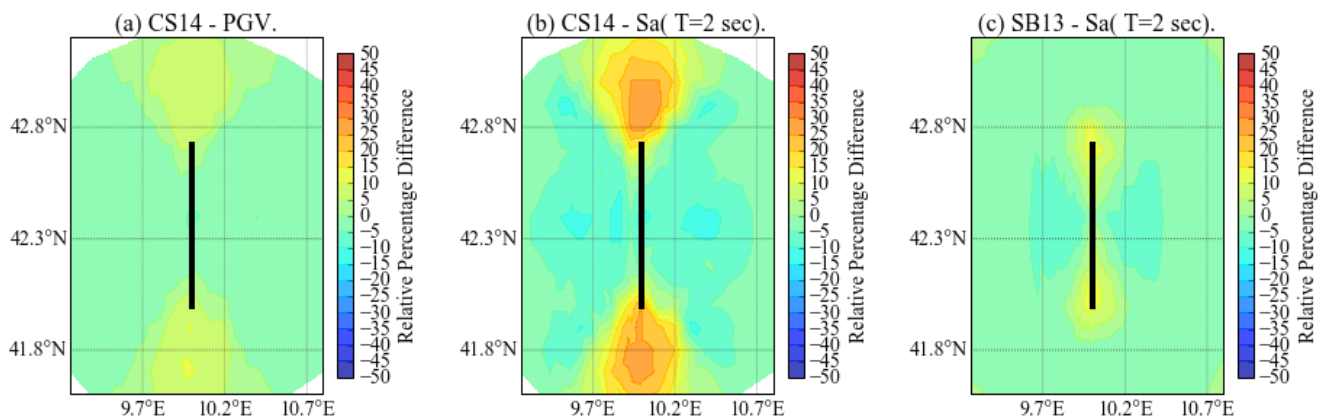


Fig. 6 - Relative percentage difference (%) of hazard map includes near-fault directivity calculation and the ordinary uniform hazard spectrum at 2% probability of exceedance (PoE) in 50 years for CS14 directivity model at PGV, Sa( T=2 sec.), and SB13 directivity model at Sa( T=2 sec.) for a strike-slip controlling scenario with the hypocenter location demonstrating in case 10 (see in Fig. 2).

Hergert et al. [21] provide a detailed description of the fault geometry this section of the North Anatolian Fault which contains 108 fault segments. Attempting to faithfully reproducing the initial fault geometrical configuration provided by Hergert et al. is impractical in the hazard calculation therefore we simplify the fault

geometry according by merging segments whose strike angle is within a prefixed threshold. If the strike angle variation between the two neighbor segment is smaller than the threshold value, then the two segments will be approximated into one segment by connecting end-to-end of the two segments. Fig. 7 demonstrates results of downsampling the fault geometry based on a threshold angle variation of 5 degrees (the fault resampled to 19 segments) and a threshold angle variation of 21 degrees (in which case the fault is resampled to a single segment). From Fig. 7, it is evident that when incorporating near-fault directivity into the seismic hazard evaluation, the result can change significantly depending on geometry of the rupture. For example, Istanbul, in the case of the simplest rupture geometry is in area where the directivity effect is de-amplifying the motion, in contrast with the patterns observed for the other test cases.

We take the result of test case obtained considering a resampling angle of 5 degrees with 19 fault segments (Fig. 8a) as reference and we compute the difference in range of mean value with  $\pm 1$  standard deviation between the reference case and the other test cases and summarized the result in Fig. 9. It is clear from the chart that when the resampling angle is less than 18 degrees (the fault geometry approximation to more than 3 segments), the result are stable and provide a sufficiently accurate near-fault directivity seismic hazard evaluation. Beyond doubt, with single segment approximation as representation of the NAF fault will result an unreliable result.

## 6. Conclusion

In this contribution, we describe the outcomes of a sensitivity analysis on the hazard results computed considering near-fault directivity effects. We find that at near-fault sites, including near-fault rupture directivity effect into PSHA is essential for computing accurate hazard values.

For a simple scenario analysis based on a planar strike-slip fault, we observe hazard levels increased up to 65% compared to the obtained considering ordinary calculations. The hypocenter location strongly dominates the spatial variation of hazard level introduced by directivity especially for scenario calculation. A second test used to explore the sensitivity of the spatial pattern of hazard shows that an over simplified geometrical structure can lead to a completely unreliable result.

The CS14 directivity model and the SB13 directivity model show significantly diverse patterns in the hazard results. A possible explanation of this difference is that the “directivity model”, described by these two models account for different phenomena (although they are related). The CS14 model predicts a global directivity effect caused by the finite fault rupture propagation effect embedded with radiation pattern with nearly uniform slip distribution and constant rupture velocity assigned. On the other hand, the SB13 model computes the ground motion considering pulse-like effects which are the result of heterogeneity in fault rupture process which the rupture path towards to the target sites passing through high-slip zones (local directivity). In the future, the more ideal approach should either apply both kinds of models introducing the spatial variation on hazard result by global directivity effect and on top of it, adding the modification of the impact from potential pulselike motions caused by local directivity effect or alternatively, make a use of logic tree framework for combining the directivity-term-included GMPEs derived by these two types of directivity models in order to cover the general near-fault rupture directivity related epistemic uncertainties in near-field ground motion prediction.

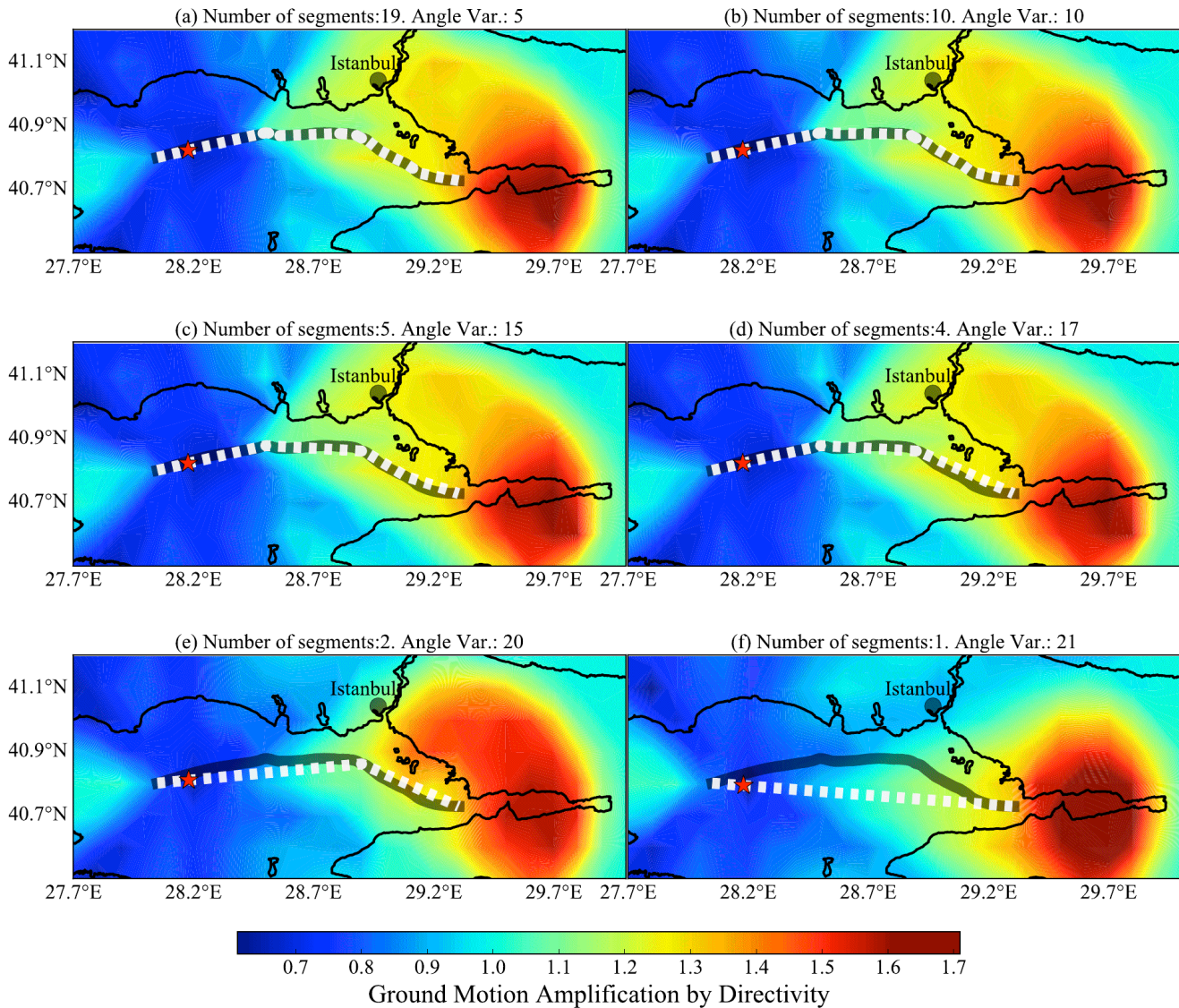


Fig. 7 – Fault geometry resampling sensitivity test. The amplification of ground motion due to rupture directivity in CY2014 GMPE by using CS14 directivity model at spectrum acceleration ( $T=5$  sec.) for various fault approximation test cases. The black traces indicates the initial fault traces provided by Hergert et al.(2011)[21]. The white dashed line shows the resampled fault trace. The black dot presents the city center of Istanbul.

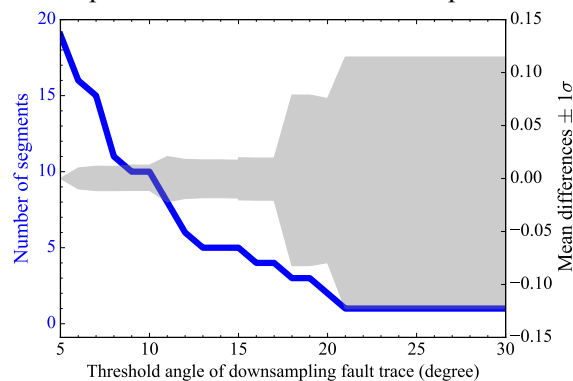


Fig. 8 - A chart demonstrates the pattern of the residuals for various fault geometry approximation assumption. Here, we take the fault resampled into 19 segments as reference (as shown in Fig. 7a).

## 5. References

- [1] Somerville PG, Smith NF, Graves RW, Abrahamson NA. (1997): Modification of Empirical Strong Ground Motion Attenuation Relations to Include the Amplitude and Duration Effects of Rupture Directivity. *Seismol. Res. Lett.*, 68(1), 199–222.
- [2] Abrahamson NA. (2000): Effects of rupture directivity on probabilistic seismic hazard analysis. *Proc. 6th Int. Conf. Seism. Zo.*
- [3] Iervolino I, Cornell CA. (2008): Probability of occurrence of velocity pulses in near-source ground motions. *Bull. Seismol. Soc. Am.*, 98(5), 2262–2277.
- [4] Spudich BP, Chiou BSJ, Graves R, Collins N, Somerville P. (2004): A Formulation of Directivity for Earthquake Sources Using Isochrone Theory. *U.S. Geol. Surv. Open-File Rept. 2004-1268*, 54.
- [5] Shahi SK, Baker JW. (2011): An empirically calibrated framework for including the effects of near-fault directivity in probabilistic seismic hazard analysis. *Bull. Seismol. Soc. Am.*, 101(2), 742–755.
- [6] Spudich P, Chiou BSJ. (2008): Directivity in NGA earthquake ground motions: analysis using isochrone theory. *Earthq. Spectra*, 24(1), 279–298.
- [7] Shahi SK. (2013): A probabilistic framework to include the effects of near-fault directivity in seismic hazard assessment. Stanford University.
- [8] Spudich P, Bayless JR, Baker J, Chiou BSJ, Rowshandel B, Shahi S, et al. (2013): Final Report of the NGA-West2 Directivity Working Group. *Pacific Eng. Res. Cent. Rep.*, (May 2013), 162.
- [9] Rowshandel B. (2009): Ground motion hazard and scenario design earthquakes including source rupture effects, case in study: City of San Francisco. *Earthq. Spectra*, 25(2), 379–414.
- [10] Tothong P, Cornell CA, Baker JW. (2007): Explicit directivity-pulse inclusion in probabilistic seismic hazard analysis. *Earthq. Spectra*, 23(4), 867–891.
- [11] Mena B, Mai PM. (2011): Selection and quantification of near-fault velocity pulses owing to source directivity. *Georisk*, 5(1), 25–43. Taylor & Francis.
- [12] Spagnuolo E, Herrero A, Cultrera G. (2012): The effect of directivity in a PSHA framework. *Geophys. J. Int.*, 191(2), 616–626.
- [13] Tothong P, Cornell CA, Baker JW. (2007): Explicit Directivity-Pulse Inclusion in Probabilistic Seismic Hazard Analysis. *Earthq. Spectra*, 23(4), 867–891. Retrieved April 27, 2016, from <http://earthquakespectra.org/doi/abs/10.1193/1.2790487>
- [14] Spagnuolo E, Faenza L, Cultrera G, Michelini A, Herrero A, Saraò A. (2010): Accounting for rupture directivity in ShakeMap. *Eur. Seismol. Comm.*
- [15] Pagni M, Monelli D, Weatherill G, Danciu L, Crowley H, Silva V, et al. (2014): OpenQuake engine: an open hazard (and risk) software for the global earthquake model. *Seismol. Res. Lett.*, 85(3), 692–702. Seismological Society of America.
- [16] Mai PM, Spudich P, Boatwright J. (2005): Hypocenter locations in finite-source rupture models. *Bull. Seismol. Soc. Am.*, 95(3), 965–980. Seismological Society of America.
- [17] Chiou B-J, Youngs RR. (2008): An NGA model for the average horizontal component of peak ground motion and response spectra. *Earthq. Spectra*, 24(1), 173–215.
- [18] Somerville PG. (2003): Magnitude scaling of the near fault rupture directivity pulse. *Phys. earth Planet. Inter.*, 137(1), 201–212. Elsevier.
- [19] Chiou BS-J, Youngs RR. (2014): Update of the Chiou and Youngs NGA model for the average horizontal component of peak ground motion and response spectra. *Earthq. Spectra*, 30(3), 1117–1153. Earthquake Engineering Research Institute.
- [20] Ancheta TD, Darragh RB, Stewart JP. : PACIFIC EARTHQUAKE ENGINEERING PEER NGA-West2 Database. (May 2013).
- [21] Hergert T, Heidbach O, Bécél A, Laigle M. (2011): Geomechanical model of the Marmara Sea region-I. 3-D contemporary kinematics. *Geophys. J. Int.*, 185(3), 1073–1089.